Stem Cell Reports
Article

ISSCR

OPEN ACCESS

Ribosome biogenesis controls cranial suture MSC fate via the complement pathway in mouse and human iPSC models

Supawadee Jariyasakulroj,[1,3,4] Wei Zhang,[1,4] Jianhui Bai,[2] Minjie Zhang,[2] Zhipeng Lu,[2] and Jian-Fu Chen[1,*]
[1]Center for Craniofacial Molecular Biology, University of Southern California, Los Angeles, CA 90033, USA
[2]Department of Pharmacology and Pharmaceutical Sciences, University of Southern California, Los Angeles, CA 90089, USA
[3]Department of Masticatory Science, Faculty of Dentistry, Mahidol University, Bangkok 10400, Thailand
[4]These authors contributed equally
*Correspondence: jianfu@usc.edu
https://doi.org/10.1016/j.stemcr.2023.10.015

SUMMARY

Disruption of global ribosome biogenesis selectively affects craniofacial tissues with unclear mechanisms. Craniosynostosis is a congenital craniofacial disorder characterized by premature fusion of cranial suture(s) with loss of suture mesenchymal stem cells (MSCs). Here we focused on ribosomopathy disease gene *Snord118*, which encodes a small nucleolar RNA (snoRNA), to genetically disturb ribosome biogenesis in suture MSCs using mouse and human induced pluripotent stem cell (iPSC) models. *Snord118* depletion exhibited p53 activation, increased cell death, reduced proliferation, and premature osteogenic differentiation of MSCs, leading to suture growth and craniosynostosis defects. Mechanistically, *Snord118* deficiency causes translational dysregulation of ribosomal proteins and downregulation of complement pathway genes. Further complement pathway disruption by knockout of complement C3a receptor 1 (*C3ar1*) exacerbated MSC and suture defects in mutant mice, whereas activating the complement pathway rescued MSC cell fate and suture growth defects. Thus, ribosome biogenesis controls MSC fate via the complement pathway to prevent craniosynostosis.

INTRODUCTION

Craniosynostosis is a craniofacial birth defect that occurs as a consequence of premature fusion of cranial sutures. Children born with craniosynostosis usually have developmental delay, facial abnormality, neurological dysfunction, and psychological disturbances. Both environmental factors and genetic variants have been identified as causing or being risk factors for this devastating disorder (Kajdic et al., 2018; Stanton et al., 2022). Loss of mesenchymal stem cells (MSCs) from the cranial suture and an imbalance between bone formation and bone resorption at the osteogenic fronts disrupt cranial suture homeostasis, leading to the premature suture fusion. Previous studies have identified multiple cranial suture MSCs, including Gli1$^+$, Axin2$^+$, and Prx1$^+$ cells (Maruyama et al., 2016; Zhao et al., 2015). Gli1$^+$ MSC loss occurs early and leads to craniosynostosis in mice (Zhao et al., 2015). Adding them back can regenerate cranial sutures, as well as mitigate skull and neurocognitive defects in craniosynostosis mice (Yu et al., 2021). Previous studies have mainly focused on signaling and transcriptional factors within suture MSCs. The function of housekeeping processes such as ribosome biogenesis in craniofacial MSCs remains poorly understood.

Ribosome biogenesis occurs in the nucleolus and is a fundamental housekeeping process universally required for mRNA translation in all cells and tissues. Emerging evidence shows that ribosome biogenesis has tissue-specific regulation and functions (Mills and Green, 2017; Yelick and Trainor, 2015). This is supported by a group of human genetic disorders called ribosomopathies, which are caused by mutations in ribosomal proteins (RPs) or ribosome biogenesis factors (Farley-Barnes et al., 2019; Khajuria et al., 2018; Mills and Green, 2017; Yelick and Trainor, 2015). Disease phenotypes of ribosomopathies are heterogeneous but tend to affect specific tissue types, including craniofacial and skeletal tissues (Hetman and Slomnicki, 2019; Mills and Green, 2017; Yelick and Trainor, 2015). Dysregulation of ribosome biogenesis or nucleolar activity has been associated with craniosynostosis (Holmes et al., 2020; Neben et al., 2014). However, the underlying cellular and molecular mechanisms by which ribosome biogenesis disruption drives craniosynostosis have yet to be established. Overall, the functional specificity of ribosome biogenesis in individual tissues remains an active research area. MSCs represent an important entry point to address this issue given their importance in craniofacial biology and diseases.

Snord118 is a small nucleolar RNA (snoRNA), a class of small RNA molecules that primarily guide chemical modifications of ribosomal RNAs (rRNAs) (Kiss et al., 2006; Kufel and Grzechnik, 2019; Stepanov et al., 2015). *Snord118* encodes the box C/D snoRNA U8 that is required for rRNA maturation and acts as a ribosome biogenesis factor (Jenkinson et al., 2016; Kiss et al., 2006; Peculis and Steitz, 1993). Here we use *Snord118* as a genetic and molecular tool to disturb ribosome biogenesis by knocking out *Snord118* in Gli1$^+$ mouse suture

MSCs as well as human iPSC-derived MSCs. MSCs with impaired ribosome biogenesis exhibited p53 activation, increased cell death, reduced proliferation, and premature osteogenic differentiation, which resulted in suture growth and craniosynostosis defects. Ribosome profiling and functional genetic studies showed that the complement pathway is a key mediator of ribosome biogenesis-mediated regulation of MSC fate.

RESULTS

Snord118 mutant mice exhibited suture growth and craniosynostosis-like defects

To investigate the functions of ribosome biogenesis in suture MSCs during calvarial growth, we used *Gli1-Cre^{ERT2}* mice, which specifically express Cre in Gli1^{+} suture MSCs (Zhao et al., 2015). We crossed *Gli1-Cre^{ERT2}* with *Snord118$^{f/f}$* mice—which have *LoxP* sites flanking the *Snord118* gene—to generate *Snord118* MSC-specific heterozygous and homozygous conditional knockout (cKO) mice. Tamoxifen was administered at postnatal day 20 (P20). Suture morphology and suture volume of *Gli1-Cre^{ERT2};Snord118$^{f/f}$* and *Gli1-Cre^{ERT2};Snord118$^{f/+}$* mice were compared with littermate control wild-type (WT) mice. Our micro-computed tomography (μCT) and histology results showed that the volume of coronal and sagittal sutures was significantly reduced in *Gli1-Cre^{ERT2};Snord118$^{f/f}$* homozygous cKO mice compared with WT controls at 1 month after tamoxifen induction (Figures 1A–1D). Sagittal suture volume decreased in mutant mice in a *Snord118* dose reduction-dependent manner (Figure 1D), while both heterozygous and homozygous cKO mice exhibited coronal suture volume reduction (Figure 1C). Coronal suture malformation in *Snord118* mutant mice resembles the phenotype in *Twist1$^{+/-}$* craniosynostosis mice. Therefore, we examined *Twist1* expression and found that *Twist1*$^{+}$ cells are significantly reduced in *Snord118* mutant coronal and sagittal sutures (Figures 1E, 1F, S1A, and 1B). To examine the relative long-term consequence of suture growth defects, we analyzed homozygous cKO mice at 3 months post-tamoxifen induction. The μCT results showed that *Snord118* loss in Gli1^{+} suture MSCs disrupts suture homeostasis and subsequently leads to craniosynostosis-like partial suture fusion defects (Figures 1G and 1H). About 75% of *Gli1-Cre^{ERT2};Snord118$^{f/f}$* mutant mice showed suture fusion defects at 3 months after tamoxifen induction; all of the *Gli1-Cre^{ERT2};Snord118$^{f/f}$* mutant mice exhibited reduced coronal and sagittal suture volume compared with controls (Figures 1I and 1J). Together, these results suggest that *Snord118*-dependent ribosome biogenesis is crucial in suture MSCs to prevent craniosynostosis defects.

Snord118 depletion leads to MSC p53 activation, cell death, proliferation reduction, and loss of mesenchymal stromal cells

Since sagittal homozygous cKO mice displayed more severe and consistent suture defects than heterozygous mice, we focused on sagittal homozygous cKO mice for the downstream phenotype analyses. It has been reported that Gli1^{+} MSC loss occurs early and causes craniosynostosis in mice (Zhao et al., 2015). To investigate the causes of suture growth and craniosynostosis defects, we examined Gli1^{+} MSCs in our *Snord118* cKO mice. Ai14 mice expressed robust tdTomato fluorescence following Cre-mediated recombination and were used to label Gli1^{+} MSCs. We generated *Gli1-Cre^{ERT2};Snord118$^{f/f}$;Ai-14* mice and administrated tamoxifen at P20. One month later we examined tdTomato-marked Gli1^{+} cells. Immunohistochemical (IHC) staining showed that Gli1-tdTomato^{+} cells were significantly reduced in *Gli1-Cre^{ERT2};Snord118$^{f/f}$;Ai-14* mice compared with controls (Figures 2A and 2C). Gli1-tdTomato^{+} cells could contain both Gli1^{+} MSCs and differentiated mesenchymal cells. To ensure Gli1^{+} MSC changes, we performed Gli1 RNAscope staining and found that the percentage of Gli1^{+} MSCs was significantly reduced in mutant sutures compared with controls (Figures S1C and S1D). Previous studies have reported that p53 is activated upon disruption of ribosomal biogenesis (Golomb et al., 2014; Jones et al., 2008). Therefore, we examined p53 and found that tdTomato-labeled Gli1^{+} MSCs exhibited a significant p53 upregulation in mutant sutures compared with controls (Figures 2B and 2D). Sustained p53 activation inhibits the cell cycle and leads to cell death. To examine cell survival, we performed TUNEL staining and found that TUNEL-positive Gli1^{+} MSCs were significantly increased after *Snord118* depletion (Figures 2E and 2G). Next, we used Ki67 to label all cycling cells and found that Ki67-positive Gli1^{+} MSCs were decreased in mutant sutures compared with controls (Figures 2F and 2H), suggesting reduced cell proliferation of Gli1^{+} MSCs after *Snord118* depletion. Cranial suture patency is maintained by mesenchymal cells, which are derived from Gli1^{+} MSCs. Suture growth and MSC loss defects in mutant mice prompted us to examine suture mesenchymal cells, which are labeled by platelet-derived growth factor receptor alpha (Pdgfrα). Consistent with Gli1^{+} MSC loss, *Snord118* cKO mice displayed a decrease in Pdgfrα^{+} mesenchymal cells (Figures 2I and 2M), including both Pdgfrα^{+};Gli1-tdTomato^{+} and Pdgfrα^{+};Gli1-tdTomato^{-} cells (Figure S2). To determine the specificity of MSC and mesenchymal cell loss, we used CD31 and βIII-Tubulin (TUBB3) to label blood vessel endothelial cells and neurons, respectively. There were no significant changes in the numbers of CD31^{+} endothelial cells and TUBB3^{+} neurons after *Snord118* deletion (Figures 2J–2L).

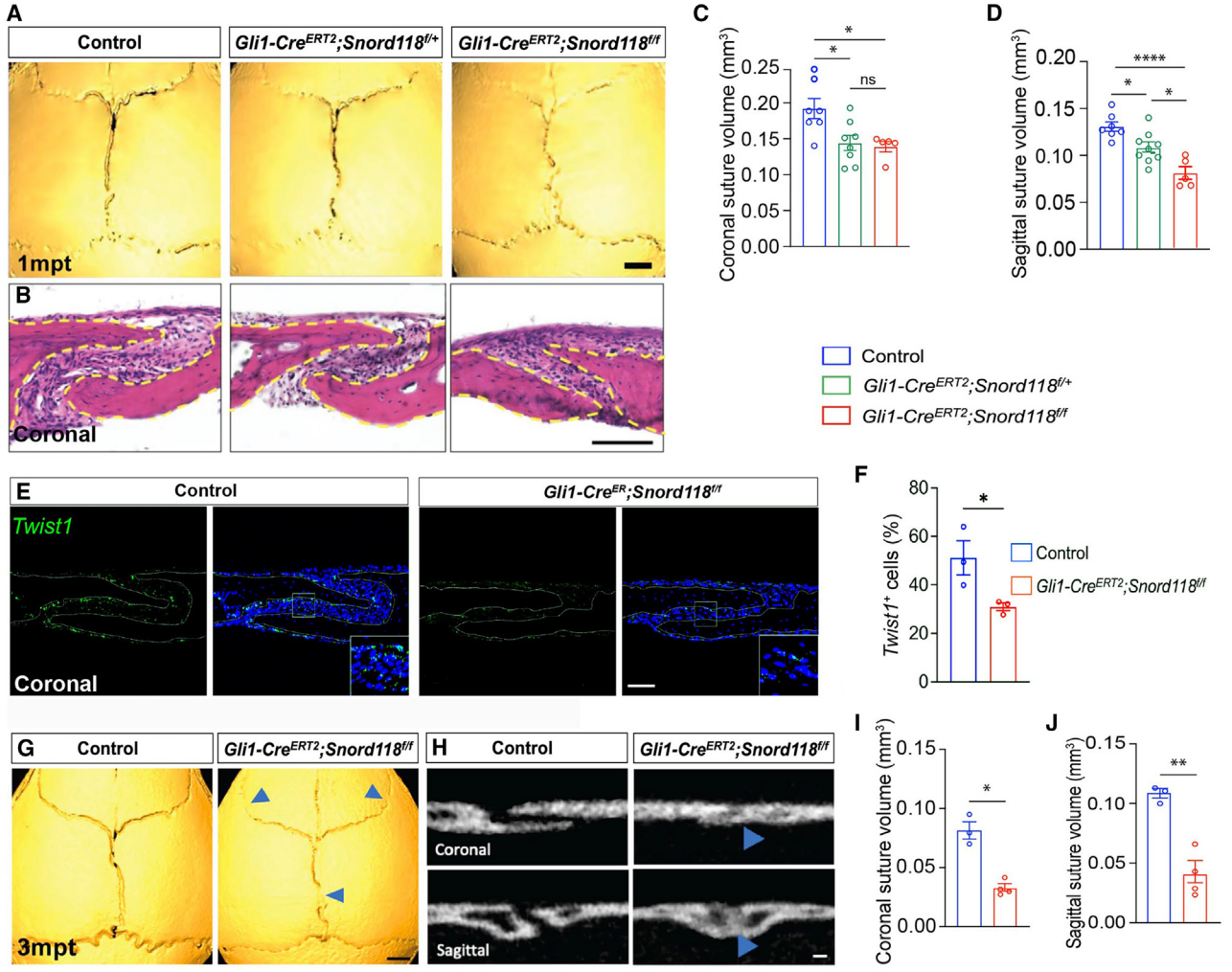

Figure 1. Ribosome biogenesis disruption in MSCs reduces suture volume and leads to craniosynostosis-like defects

(A and B) Micro-CT analysis and H&E staining of coronal and sagittal sutures from WT control, *Gli1-Cre*^{ERT2}*;Snord118*$^{f/+}$, and *Gli1-Cre*^{ERT2}*;Snord118*$^{f/f}$ skulls at 1 month post-tamoxifen administration (1 mpt). Scale bars, 1 mm (A), 100 μm (B).

(C and D) Quantification of coronal and sagittal suture volume.

(E) RNAscope staining of *Twist1* (green) in the coronal suture with tamoxifen induction at P20. Hoechst stains nuclei (blue). Scale bar, 100 μm.

(F) Quantification of the percentage of *Twist1*$^{+}$ cells in the coronal suture mesenchyme per section.

(G and H) Micro-CT analysis of control and *Gli1-Cre*^{ERT2}*;Snord118*$^{f/f}$ mice 3 months post-tamoxifen administration (3 mpt). Blue arrowheads indicate the area of partial suture fusion.

(I and J) Quantification of the volume of sagittal and coronal sutures from control and *Gli1-Cre*^{ERT2}*;Snord118*$^{f/f}$ mice (3 mpt). Scale bars, 1 mm (G), 50 μm (H). Values represent mean ± SEM with statistical significance assessed by Student's t tests and one-way ANOVA with Tukey post hoc tests (n = 3–8 mice). *p < 0.05, **p < 0.01, ****p < 0.0001; ns represents nonsignificant.

Gli1 is broadly expressed in diverse types of cells in development and is gradually restricted to the cranial suture region from P21 to 1-month-old mice (Zhao et al., 2015). To investigate ribosome biogenesis specifically in Gli1^{+} MSCs, we administrated tamoxifen to deplete *Snord118* in Gli1^{+} MSCs in 1-month-old mutant mice. Staining results showed that the percentage of Gli1^{+} MSCs is significantly reduced in mutant sutures (Figures S3A and S3B). Mutant cranial sutures exhibited p53 upregulation (Figures S3C and S3D), increased TUNEL^{+} cells (Figures S3E and S3F), and decreased Ki67^{+} cells (Figures S3G and S3H) compared with controls. Together, these results suggest that *Snord118* depletion-induced ribosome biogenesis perturbation in Gli1^{+} MSCs activates p53, causes cell death, proliferation reduction, and mesenchymal stromal/stem cell loss, leading to cranial suture growth and craniosynostosis defects.

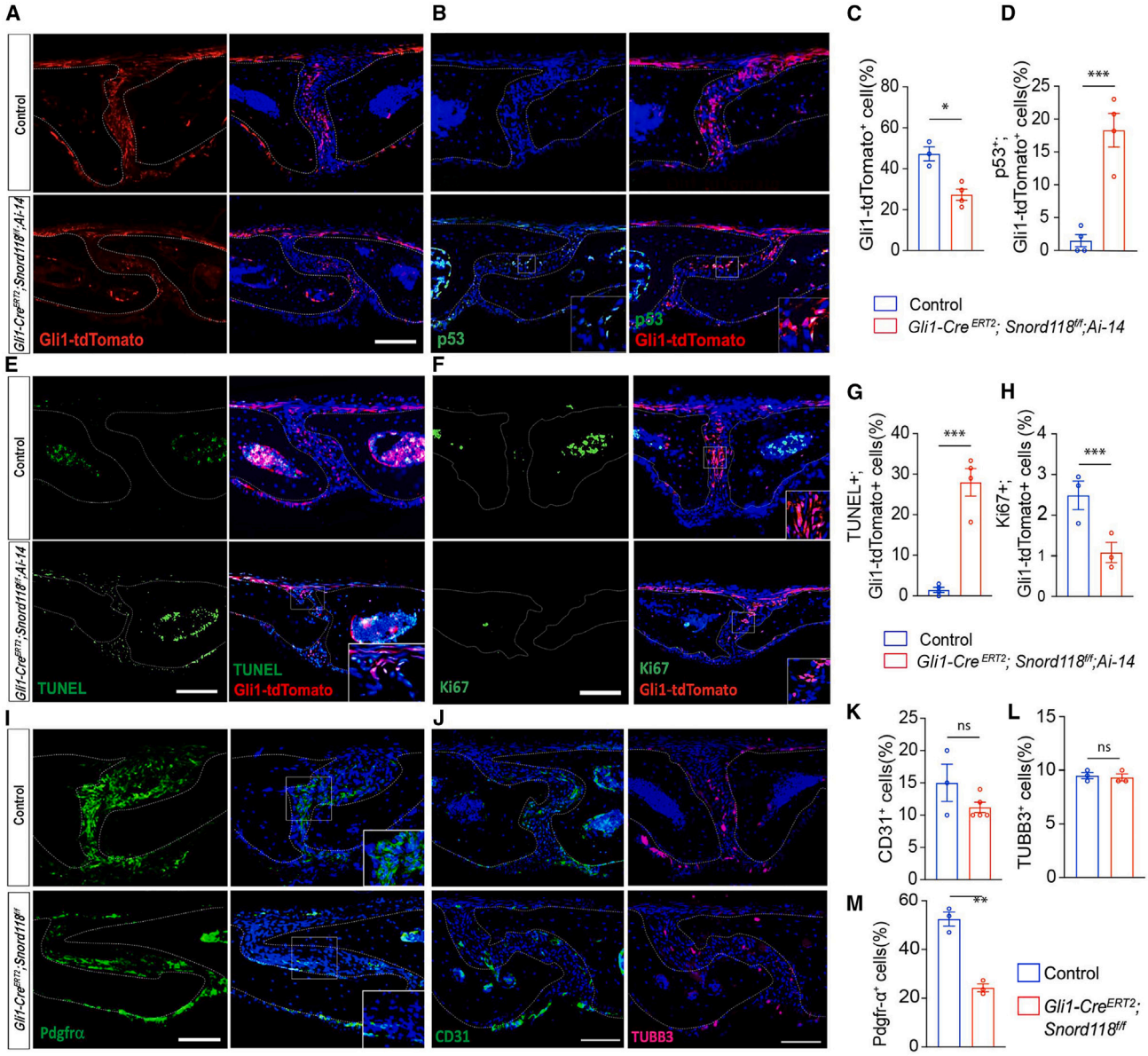

Figure 2. *Snord118* depletion leads to MSC p53 activation, cell death, proliferation reduction, and loss of mesenchymal stromal cells

Gli1-Cre^{ERT2};Ai-14 mice were used to genetically label Gli1$^+$ suture MSCs, followed by confocal imaging of sagittal sutures after IHC staining. Hoechst stains nuclei (blue).

(A and B) IHC staining of Gli1-tdTomato suture MSCs with or without co-staining p53.

(C and D) Quantification of the percentage of Gli1-tdTomato$^+$ cells and p53$^+$;Gli1-tdTomato$^+$ cells in the suture mesenchyme per section.

(E and F) TUNEL and Ki67 IHC staining cells with or without Gli1-tdTomato.

(G and H) Quantification of the percentage of TUNEL- or Ki67-positive Gli1-tdTomato$^+$ cells per section.

(I and J) IHC staining of Pdgfrα, CD31, and TUBB3.

(K–M) Quantification of the percentage of Pdgfrα$^+$, CD31$^+$, and TUBB3$^+$ cells per section. Scale bars, 100 μm. Values represent mean ± SEM with statistical significance assessed by Student's t tests (n = 3–4 mice). *p < 0.05, **p < 0.01, ***p < 0.001, ****p < 0.0001; ns represents nonsignificant.

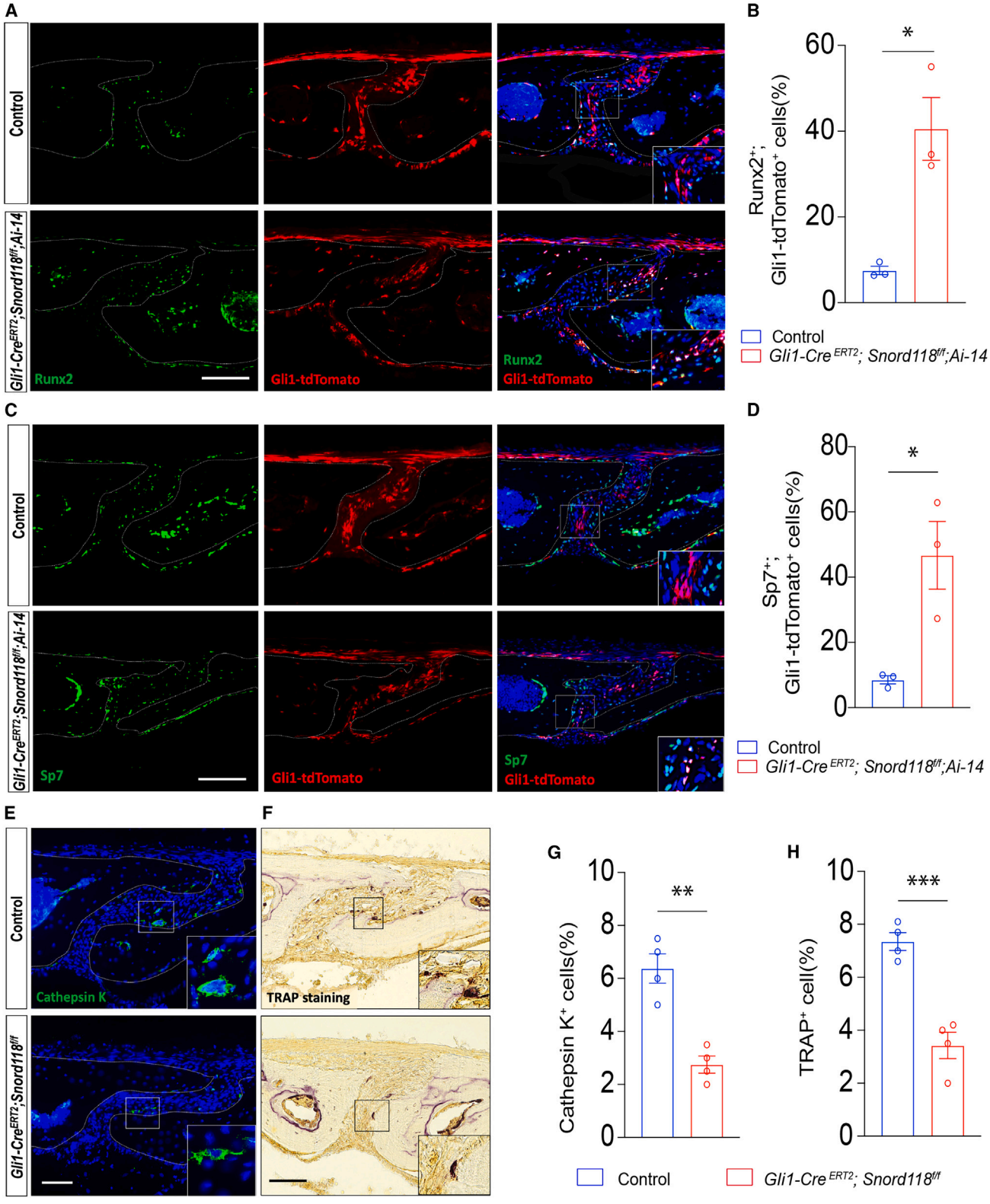

(legend on next page)

Snord118 depletion leads to the premature osteogenic differentiation of MSCs and osteoclast loss

In addition to cell survival, we investigated how ribosome biogenesis disruption affects other cell behaviors of Gli1$^+$ MSCs. Gli1$^+$ MSCs can differentiate into the osteoblast lineage (Zhao et al., 2015). Transcription factor Runx2 marks preosteoblast cells and is indispensable for osteoblast differentiation during both endochondral and intramembranous ossification. Sp7 is a zinc finger-containing transcription factor acting downstream of Runx2 and is essential for osteoblast differentiation and bone formation (Nakashima et al., 2002). Consistent with Gli1$^+$ MSC loss, the total osteoblast cells marked by Runx2 or Sp7 appear fewer in mutant cranial sutures compared with controls (Figures 3A and 3C). To monitor the differentiation of individual MSCs into osteoblast cells, we lineage traced tdTomato-positive Gli1$^+$ MSCs and found that the percentage of Runx2-and tdTomato-Gli1-double-positive cells are significantly increased in the mutant cranial sutures compared with controls (Figure 3B). Similarly, Sp7- and tdTomato-Gli1-double-positive cells were increased in mutant cranial sutures as well (Figure 3D). In addition, *Snord118* depletion in Gli1$^+$ MSCs in 1-month-old mice resulted in an increase in the percentage of Runx2$^+$ or Sp7$^+$ Gli1 MSCs (Figure S4).

Cranial suture homeostasis is maintained by the interaction of MSCs with their niche cells, which keeps the balance between osteogenesis and osteoclastogenesis. Disruption of the bone remodeling process, including osteoclast-mediated bone resorption in the suture, can lead to craniosynostosis. Therefore, we examined bone turnover at the osteogenic front, focusing on osteoclasts. Tartrate-resistant acid phosphatase (TRAP) and Cathepsin K were used to mark osteoclasts. IHC staining showed that the percentage of Cathepsin K-positive cells is significantly reduced in mutant cranial sutures (Figures 3E and 3G). In parallel, the TRAP-positive osteoclast cells were decreased at the osteogenic fronts of the skull in *Snord118* cKO mice compared with controls (Figures 3F and 3H). Osteoclasts originate from hematopoietic stem cells (HSCs) or erythro-myeloid progenitors (EMPs) but not from Gli1$^+$ MSCs (Yahara et al., 2022). The osteoclast reduction in mutant sutures implies a non-cell autonomous role of ribosome biogenesis in suture MSCs. Together, these findings suggest that *Snord118* depletion in Gli1$^+$ MSCs results in the premature differentiation of MSCs into osteoblasts as well as decreased osteoclast-driven bone resorption, which could collectively contribute to suture growth defects and craniosynostosis.

Human iPSC-derived mesenchymal stem cells exhibit impaired self-renewal and differentiation

To investigate the cell autonomous roles of *Snord118* in MSCs, we established a platform to differentiate human iPSCs into suture human iPSC-derived mesenchymal stem cells (iMSCs). Our *Snord118* cKO mice exhibited consistent and dose-dependent growth defects in sagittal sutures, which are derived from cranial neural crest cells (cNCCs) in early development. Therefore, we focused on cNCC-derived suture MSCs. We first directed iPSCs into cNCCs via two methods (Figure 4A), which are not significantly different in the cNCC outcomes. In the first method, we activated WNT signaling activities using 1 μM CHIR99021 (a glycogen synthase kinase-3β inhibitor to promote WNT signaling) and simultaneously inhibited SMAD signaling using 10 μM SB431543 (an inhibitor of transforming growth factor [TGF]β signaling) in human iPSCs. This resulted in a highly enriched cNCC population (Faal et al., 2019; Stebbins et al., 2019). In the second method, human iPSCs were used to generate embryonic bodies (EBs), which were then cultured in N2B27 medium in the presence of insulin, epidermal growth factor (EGF), and basic fibroblast growth factor (bFGF) on uncoated dishes without Matrigel (Bajpai et al., 2010). Under these culture conditions, neural progenitor cells detached from uncoated culture dishes and were washed away, resulting in highly purified NCCs attached to cultured dishes. Then we used an α-MEM medium in the presence of fetal bovine serum (FBS) to generate GLI1$^+$ MSCs (Figures 4A and 4B). Together, human iPSC-derived MSCs allowed us to have sufficient materials for ribosome profiling.

Using CRISPR-Cas9 approaches, we generated three independent iPSC lines with heterozygous *SNORD118* mutations, since homozygous mutations led to cell death without the production of stable iPSC lines. DNA sequencing identified specific nucleotide deletion (Figure S5A). RT-PCR confirmed *SNORD118* RNA downregulation in mutant iPSCs (Figure S5B). Single-cell clonal

Figure 3. *Snord118* depletion leads to premature osteogenic differentiation of MSCs and osteoclast loss

(A and C) Confocal imaging of sagittal sutures after IHC staining of Runx2 and Sp7 from *Gli1-Cre^{ERT2};Ai-14* (control) and *Gli1-Cre^{ERT2};Snord118$^{f/f}$;Ai-14* mice.

(B and D) Quantification of the percentage of Runx2$^+$- or Sp7$^+$-Gli1-tdTomato$^+$ cells per section. Hoechst stains nuclei (blue).

(E and F) IHC staining of Cathepsin K (left panels) and TRAP staining (right panels) in the suture mesenchyme of wild-type (WT) and *Gli1-Cre^{ERT2};Snord118$^{f/f}$* mice.

(G and H) Quantification of the percentage of Cathepsin K$^+$ cells and TRAP$^+$ cells in the suture mesenchyme per section. Scale bars, 100 μm. Values represent mean ± SEM with statistical significance assessed by Student's t tests (n = 3–4 mice). *p < 0.05, **p < 0.01, ***p < 0.001.

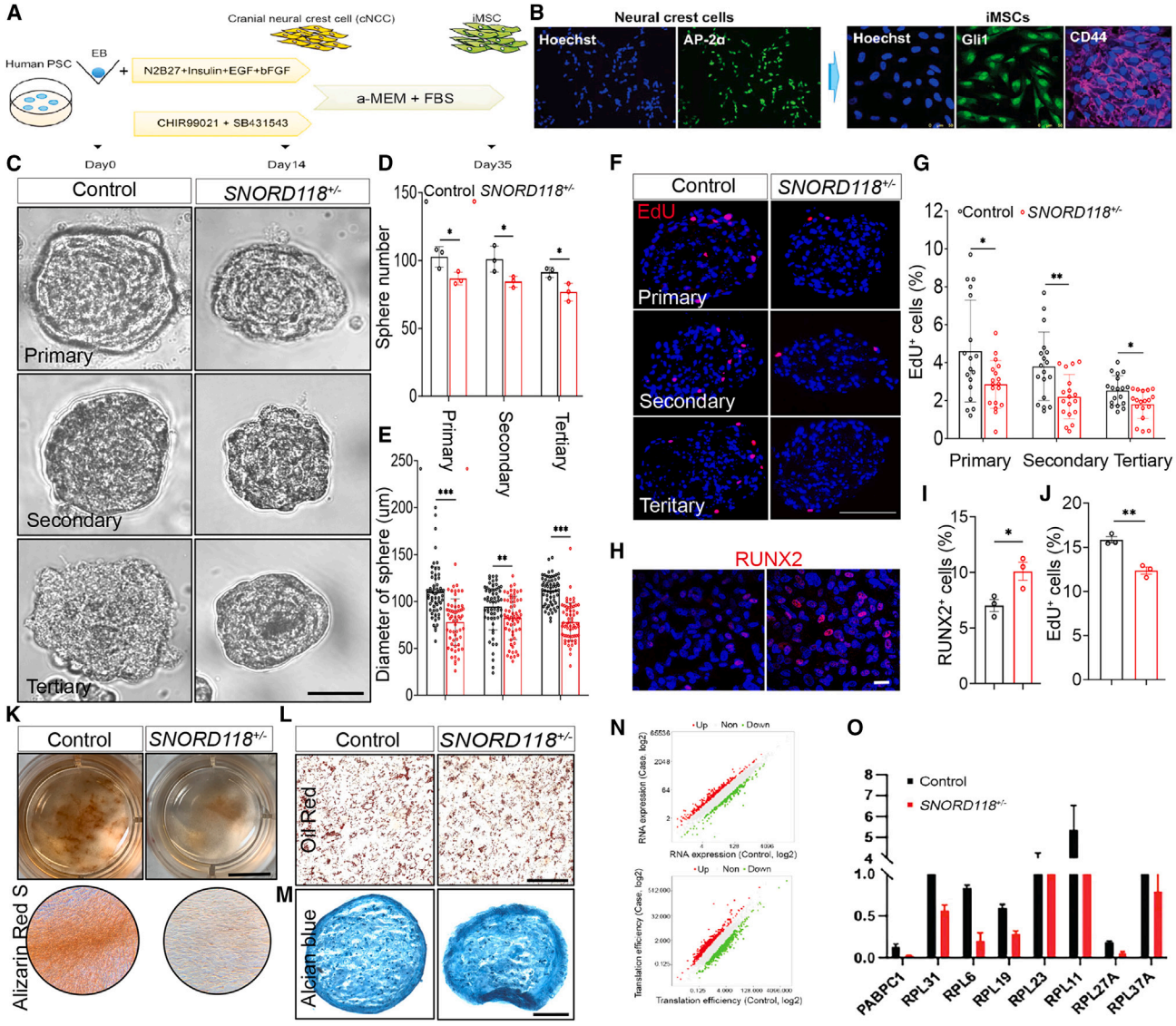

Figure 4. Mutant iPSC-MSCs exhibit impaired self-renewal, differentiation, and translational dysregulation of ribosomal protein genes

(A) Diagram of procedures of induced MSC (iMSC) generation from human iPSCs via cranial neural crest cells (cNCCs).

(B) Immunostaining of iPSC-derived NCCs and iMSCs.

(C) Bright-field images of spheres formed from control and *SNORD118*$^{+/-}$ iPSC-derived iMSCs. Scale bar, 100 μm.

(D and E) Quantification of the number of spheres from iMSCs starting with 1 × 10^4 cells and sphere diameter. N = 60 spheres analyzed for three independent cell lines with or without *SNORD118*$^{+/-}$.

(F) Representative images of EdU incorporation in the spheres. Hoechst stains nucleus (blue). Scale bar, 100 μm.

(G) Quantification of the percentage of EdU$^+$ cells in spheres. n = 18 spheres analyzed for each group.

(H) Representative images of RUNX2 staining under iMSC osteogenic differentiation at day 3. Hoechst stains nucleus (blue). Scale bar, 50 μm.

(I and J) Quantification of the percentage of RUNX2$^+$ cells or EdU+ cells in a 2D culture of iMSCs.

(K) Representative images of Alizarin Red S staining for iMSCs at osteogenic differentiation day 21. Scale bar, 1 cm.

(L and M) Representative images of adipogenic differentiation (Oil red O staining, top) and chondrocyte differentiation (Alcian blue staining, bottom) for iMSCs at differentiation day 14. Scale bar, 100 μm.

(N) Correlation between mutant iPSC-MSCs and controls in mRNA expression and translation efficiency.

(O) Analysis of RNA-seq data from total mRNAs and ribosome-protected RNAs reveals translational downregulation of genes encoding ribosomal proteins (RPs) in mutant iPSC-MSCs. n = 3 different independent iPSC lines containing control and *SNORD118*$^{+/-}$ for the generation of iMSCs. Data are mean ± SEM. *p < 0.05, **p < 0.01, ***p < 0.001, Student's t test.

analysis showed that iMSCs can effectively self-renew to form spheres. After 14 days, the spheres were dissociated and seeded as the single-cell suspension for the culture of the next passage. *SNORD118*$^{+/-}$ mutant iMSCs displayed a significant decrease in the sphere numbers out of 1 × 10^4 single cells as well as in the diameter of the spheres at the primary, secondary, and tertiary passages (Figures 4C–4E). EdU labeling showed that there was a reduced percentage of EdU$^+$ cells in the mutant spheres compared with controls (Figures 4F and 4G), which is consistent with decreased self-renewal in mutant iMSCs. The 2D culture also identified a decrease in EdU$^+$ cells in mutant iMSCs compared with controls (Figures 4J and S5D). We examined iMSC at osteogenic differentiation day 3 and found that mutant iMSCs have an increased percentage of RUNX2$^+$ cells (Figures 4H and 4I), suggesting premature osteogenic differentiation. To examine the multipotency of iMSCs, we performed tri-lineage differentiation. Alizarin Red S (ARS) staining showed that *SNORD118*$^{+/-}$ mutant cells have reduced calcium deposit in osteogenic differentiation (Figure 4K). Oil Red staining and Alcian blue staining were used to assay adipogenesis and chondrogenesis, respectively, and failed to reveal substantial differences between control and mutant cells (Figures 4L and 4M). Together, these results suggest that *SNORD118*$^{+/-}$ mutant iMSCs exhibit impaired self-renewal and osteogenic differentiation *in vitro*.

Ribosome profiling revealed a translational downregulation of RP genes in mutant MSCs

To investigate the molecular mechanisms underlying the cell fate changes of mutant MSCs, we examined translational regulation using ribosome profiling (Ingolia et al., 2019). This approach compares the levels of ribosome-protected fragments (RPFs) to the total expression levels of mRNA in individual genes to measure translational efficiency. Ribosome profiling requires a substantial number of MSCs that is technically challenging to obtain in mice. Therefore, we used our human iPSC-derived iMSCs.

To establish ribosome profiling, we titrated RNase concentrations and recovered ribosome-protected mRNA fragments for sequence library construction. RiboToolkit was used for the analysis and annotation of ribosome profiling data to decode mRNA translation at codon resolution (Liu et al., 2020). First, we examined the basic statistics of RPFs and found there were 97.06% cleaned RPFs (Figure S6A), which excludes contamination from other RNAs such as rRNA, tRNA, and snoRNA. About 18.17% of cleaned RPFs could be mapped back to the human genome (Figure S6B). We calculated 26–34 nt RPFs and found that 27–28 nt have the highest percentage (Figure S6C). These RPFs, which are about 6.7 million reads, are mainly distributed on protein-coding genes (Figure S6D). They are enriched in coding sequences (CDS) in comparison with 5′ UTR, 3′ UTR, intron, and intergenic regions (Figure S6E), which is also reflected by randomly selected GAPDH and ACTB genes (Figure S6F). Next, we examined our Ribo-seq quality by statistically analyzing the distribution of RPF coding frames including frames 0, 1, and 2. Frame 0 had the highest percentage in CDS (Figure S6G) and the RPF metagene plot around translation start sites for P-site inference (five primers to start codon: 11, 12, 12 for 26 nt, 27 nt, 28 nt size; five primers to stop codon: 15, 15, 15 for 26 nt, 27 nt, 28 nt size) (Figure S6H). Last, we examined a metagene view of the start codon using P-site offsets and found that the peaks overlap with start and stop codons (Figure S6I). These results suggest that we have successfully established ribosome profiling methodology using human iPSC-MSCs.

We differentiated mutant and isogenic control iPSC lines into iMSCs, followed by ribosome profiling. Using RiboToolkit for decoding mRNA translation (Liu et al., 2020), we compared the levels of RPFs over total mRNA between control and mutant iPSC-MSCs (Figure 4N). Bioinformatic analysis found that the top translational downregulated genes encode RPs, although the mRNA levels are relatively normal (Figures 4O and S5C). These results suggest that RPs are co-regulated at the translational level to maintain RP stoichiometry, which is consistent with findings in human hematopoiesis that ribosome levels co-translationally regulate RPs (Khajuria et al., 2018).

Transcriptional dysregulations of genes encoding complement pathway components after *Snord118* deletion

We next analyzed transcriptional dysregulation in mutant iMSCs and found that *SNORD118* mutations lead to the downregulation of complement pathway genes, including *C1S*, *C1R*, and *C1RL* in iPSC-derived MSCs (Figure 5A). Clinical genetics have shown that mutations in complement pathway components in humans selectively affect craniofacial structure. Specifically, mutations in *MASP1/3* and *COLEC10/11* cause 3MC syndrome (Mingarelli, Malpeuch, Michels, and Carnevale syndrome) with craniosynostosis, cleft lip/palate, or facial dysmorphism (Munye et al., 2017; Rooryck et al., 2011). However, the molecular and cellular mechanisms underlying craniosynostosis in 3MC syndrome remain unknown. Therefore, we carried out in-depth studies of the complement pathway. Western blots (WBs) confirmed that mutant iPSC-MSC cells have reduced protein levels in *MASP1* (Figures 5B and 5C), the mutation of which leads to 3MC syndrome. Simultaneously, there were no significant mRNA expression level changes in *MASP1* (Figure 5D), suggesting a potential translational dysregulation of MASP1 in mutant iPSC-MSCs. In addition, WBs and RT-PCR confirmed protein and mRNA

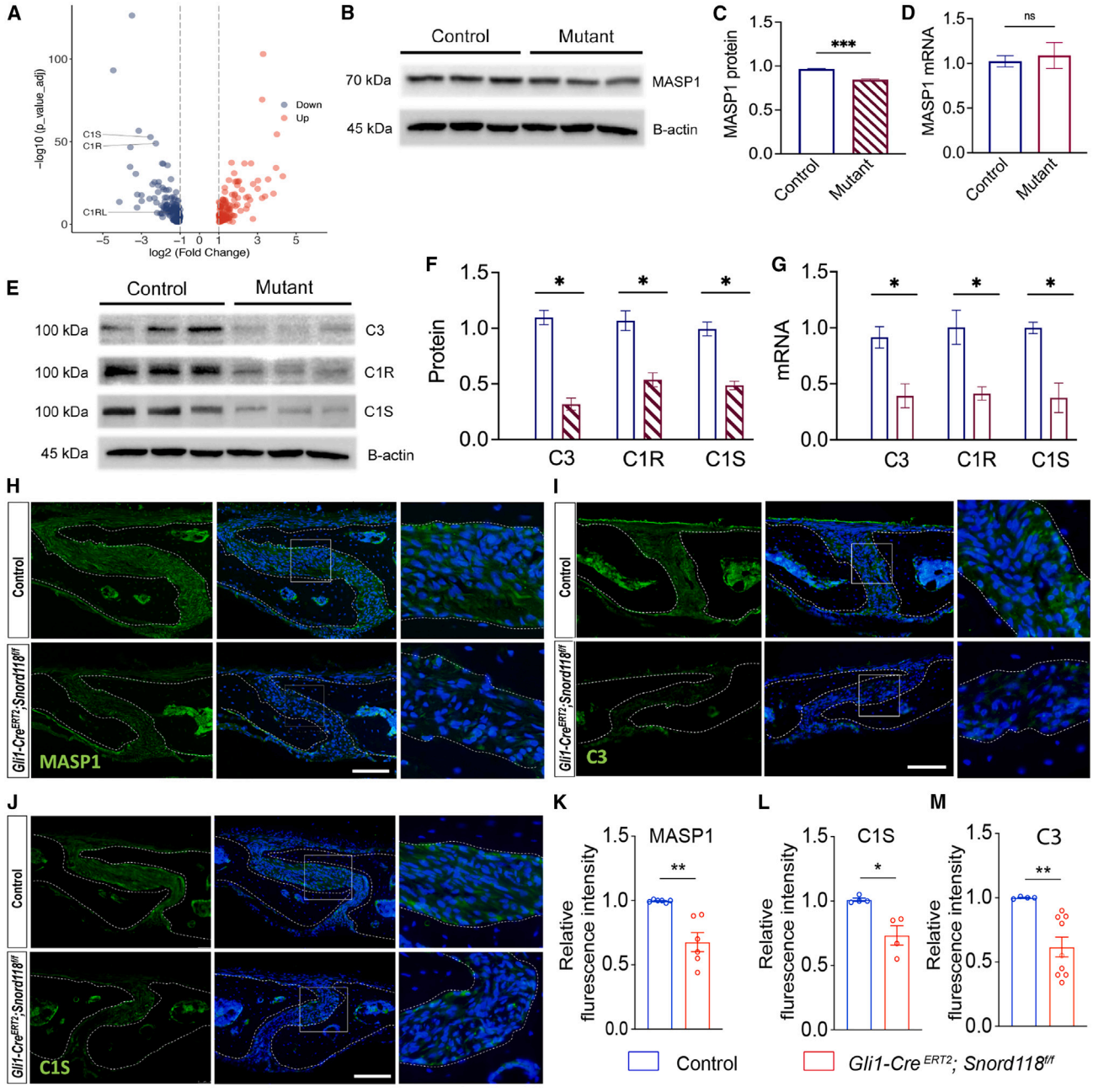

Figure 5. Transcriptional and translational dysregulation of the complement pathway in mutant iPSC-MSCs

(A) Log2-fold changes in up- and downregulated genes from bulk RNA-seq reads in the control and *SNORD118*$^{+/-}$ iMSCs. The downregulated C1S, C1R, and C1RL in mutant iMSCs are highlighted.

(B and E) Western blot (WB) analyses of protein levels of MASP1, C3, C1R, and C1S in control and *SNORD118* mutant iPSC-MSCs. β-actin serves as the negative control.

(C and F) Quantification of WB results.

(D and G) RT-PCR and quantification of mRNA levels of MASP1, C3, C1R, and C1S in control and *SNORD118* mutant iPSC-MSCs.

(H–J) Immunostaining of complement pathway proteins MASP1, C1S, and C3 in the sagittal suture mesenchyme of control and *Gli1-Cre*^{ERT2}*;Snord118*$^{f/f}$ mice.

(K–M) Quantification of relative fluorescence intensity of complement proteins. Scale bars, 100 μm. Values represent mean ± SEM with statistical significance assessed by Student's t tests (n = 3–9 biological replicates). *p < 0.05, **p < 0.01, ***p < 0.001; ns represents nonsignificant.

downregulation of complement pathway components C3, C1R, and C1S (Figures 5E–5G). To examine complement pathway dysregulations *in vivo*, we examined *Snord118* MSC cKO mice. IHC staining revealed that *Snord118*-deficient sutures exhibited a decrease in the expression of complement pathway components, including MASP1, C1S, and C3 (Figures 5H–5M). Together, these results indicate that *Snord118* deficiency leads to transcriptional dysregulation of genes in the complement pathway.

Complement pathway disruption exacerbates suture defects in *Snord118* mutant mice

Previous studies have found that the complement pathway plays a regulatory role in bone metabolism (Mödinger et al., 2018). MSCs, osteoblasts, and osteoclasts can generate C3 and express C3a receptor 1 (C3aR1). The C3a/C3aR axis is a central component of the complement pathway, which mediates the bidirectional communication between osteoclasts and osteoblasts for bone homeostasis (Mödinger et al., 2018). To examine the functional importance of the complement pathway in mediating *Snord118* functions during suture homeostasis, we performed loss-of-function perturbation using a *C3aR1* KO mouse model, which by itself has no suture growth defect or craniosynostosis. We generated *C3aR1* genetic deletion in *Snord118* MSC cKO mice by crossing *Gli1-Cre^{ERT2};Snord118$^{f/+}$* mice with *C3aR1$^{-/-}$* mice. Suture morphology and suture volume of double KO mice were compared with WT and *Gli1-Cre^{ERT2};Snord118$^{f/+}$* heterozygous mice. Compared with WT controls, heterozygous KO mice exhibited a decrease in coronal and sagittal suture volumes, which were further exacerbated by the deletion of *C3aR1* (Figures 6A–6D). These histological data were further validated by μCT analysis (Figure 6B). Our results suggest that there is a genetic interaction between *C3ar1* and *Snord118* in suture growth. To investigate the cellular basis of *C3ar1* deletion-induced exacerbation of suture defects in *Snord118* cKO mice, we examined Gli1$^+$ MSCs. We did not detect notable defects in Gli1$^+$ MSCs in *C3aR1$^{-/-}$* KO mice (data not shown), which is consistent with their normal suture growth. In contrast, complement pathway disruption by *C3aR1$^{-/-}$* deletion induced a drastic reduction of Gli1$^+$ MSCs in *Gli1-Cre^{ERT2};Snord118$^{f/+}$* heterozygous KO mice (Figures 6E and 6F). To investigate the causes of this Gli1$^+$ MSC loss, we examined p53 activation and found that there is a substantial increase in the percentage of p53-positive cells in the cranial sutures of double mutant mice compared with single KO ones and WT controls (Figures 6G and 6H). Lastly, cranial sutures exhibited an increase of TUNEL-positive cells in double mutant mice compared with single KO ones and WT controls (Figures 6I and 6J), suggesting that increased cell death underlies the MSC loss. Together, these results indicate that complement pathway disruption by *C3aR1$^{-/-}$* KO exacerbates MSC cellular defects and leads to more severe suture defects in *Snord118* cKO mice.

Complement pathway activation rescues suture defects in *Snord118* mutant suture explants

To further examine functions of the complement pathway, we investigated whether activation of the complement pathway could restore cellular behaviors and thereby rescue suture growth in *Snord118* homozygous cKO mice. To this end, a C3aR agonist was used to promote functions of the complement pathway. In order to exclude C3aR agonist-induced complications in other non-suture organs, we selected a suture explant *ex vivo* culture model, which has been well-established to study suture growth in postnatal but not adult stages (Menon et al., 2021). Coronal and sagittal sutures explanted from postnatal day 4 (P4) WT and *Gli1-Cre^{ERT2};Snord118$^{f/f}$* mice were treated with C3aR agonist for 10 days before histology analyses. WT sutures remained patent, while mutant cranial sutures showed bony fusions (Figure 7A). Importantly, agonist-treated sutures from *Snord118* cKO mice remained patent, suggesting complement pathway activation can rescue suture growth defects. Statistical analysis showed that C3aR agonist-mediated complement pathway promotion can partially rescue the suture growth defects in *Snord118* cKO mice (Figures 7B and 7C). To investigate the cellular basis of C3aR agonist's beneficial effects, we used tdTomato Ai14 mice to genetically label Gli1$^+$ MSCs and found that the C3aR agonist significantly restored MSC loss in *Snord118* cKO mice (Figures 7D and 7E). When treated with the C3aR agonist, the percentage of p53-positive suture cells was significantly reduced in mutant suture explants compared with *Gli1-Cre^{ERT2};Snord118$^{f/f}$* mutant explants treated with DMSO controls (Figures 7F and 7G). Both WT and C3aR agonist-treated mutant suture explants showed minimal cell death revealed by TUNEL staining, whereas untreated *Snord118* mutant sutures had a significant increase in cell apoptosis (Figures 7H and 7I). Therefore, the activation of the complement pathway partially rescued cellular and suture growth defects caused by *Snord118* deletion. Together, these results suggest that the complement pathway is a key mediator of *Snord118* function in MSC behaviors and suture homeostasis.

DISCUSSION

Ribosome biogenesis is a fundamental biological process, which is universally required in all eukaryotic cells. How ribosome biogenesis disruption preferentially affects craniofacial tissues, leading to craniofacial deformities, remains poorly understood. Here we found that global

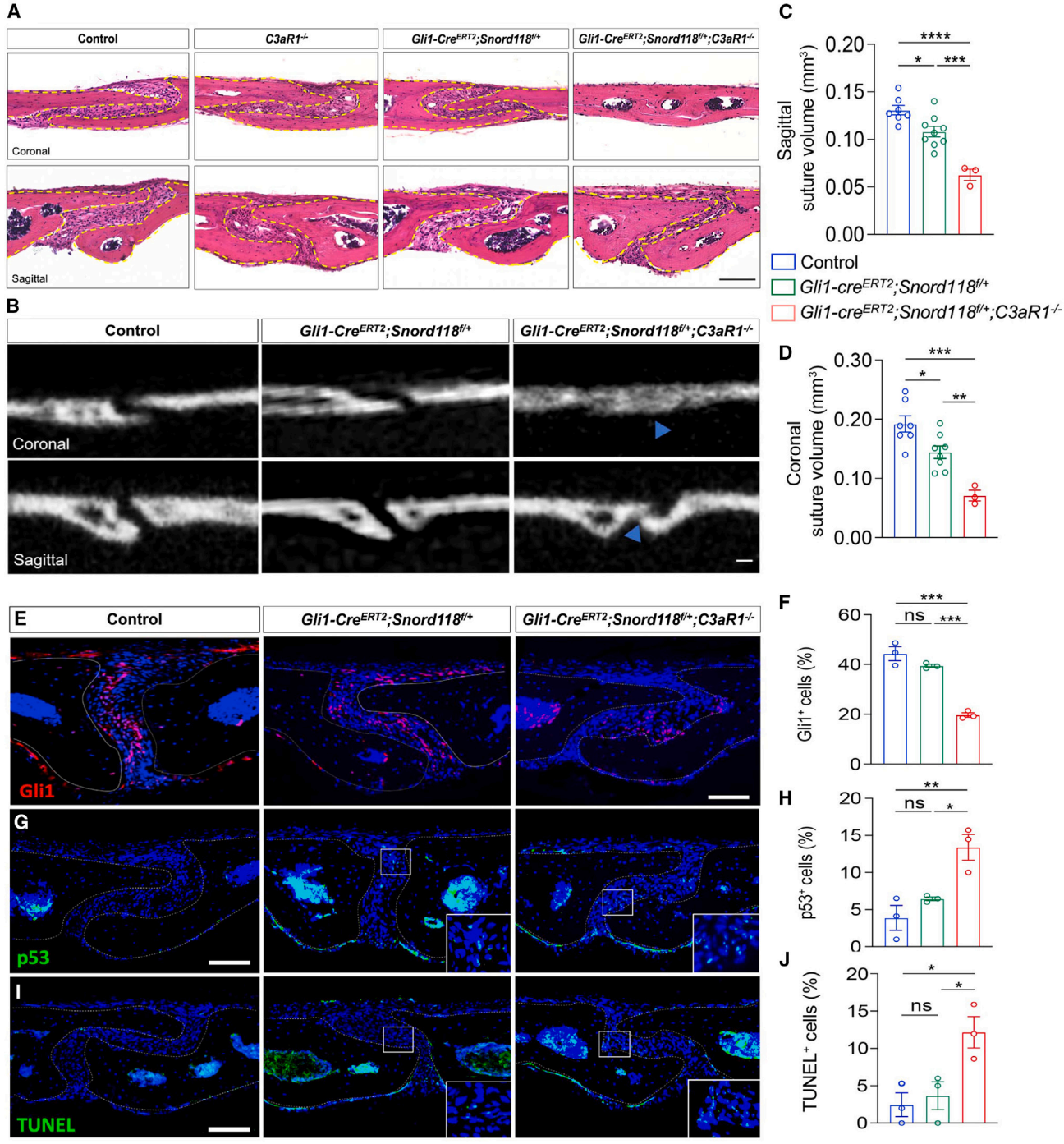

Figure 6. Complement pathway disruption exacerbates suture defects in *Snord118* mutant mice

(A) H&E staining of coronal and sagittal sutures from control, *C3aR1*$^{-/-}$, *Gli1-Cre*^{ERT2};*Snord118*$^{f/+}$, and *Gli1-Cre*^{ERT2};*Snord118*$^{f/+}$;*C3aR1*$^{-/-}$ mice.

(B) Micro-CT analysis. Scale bar, 50 um.

(C and D) Quantification of sagittal and coronal suture volume.

(E, G, and I) Confocal imaging of sagittal suture mesenchymal cells after IHC staining of Gli1 and p53 as well as TUNEL in control, *Gli1-Cre*^{ERT2};*Snord118*$^{f/+}$, and *Gli1-Cre*^{ERT2};*Snord118*$^{f/+}$;*C3aR1*$^{-/-}$ mice.

(F, H, and J) Quantification of the percentage of Gli1^{+}, p53^{+}, and TUNEL^{+} cells per section. Scale bars, 100 μm. Values represent mean ± SEM with statistical significance assessed by one-way ANOVA with Tukey post hoc tests (n = 3–5 mice). *p < 0.05, **p < 0.01, ***p < 0.001, ****p < 0.0001; ns represents nonsignificant.

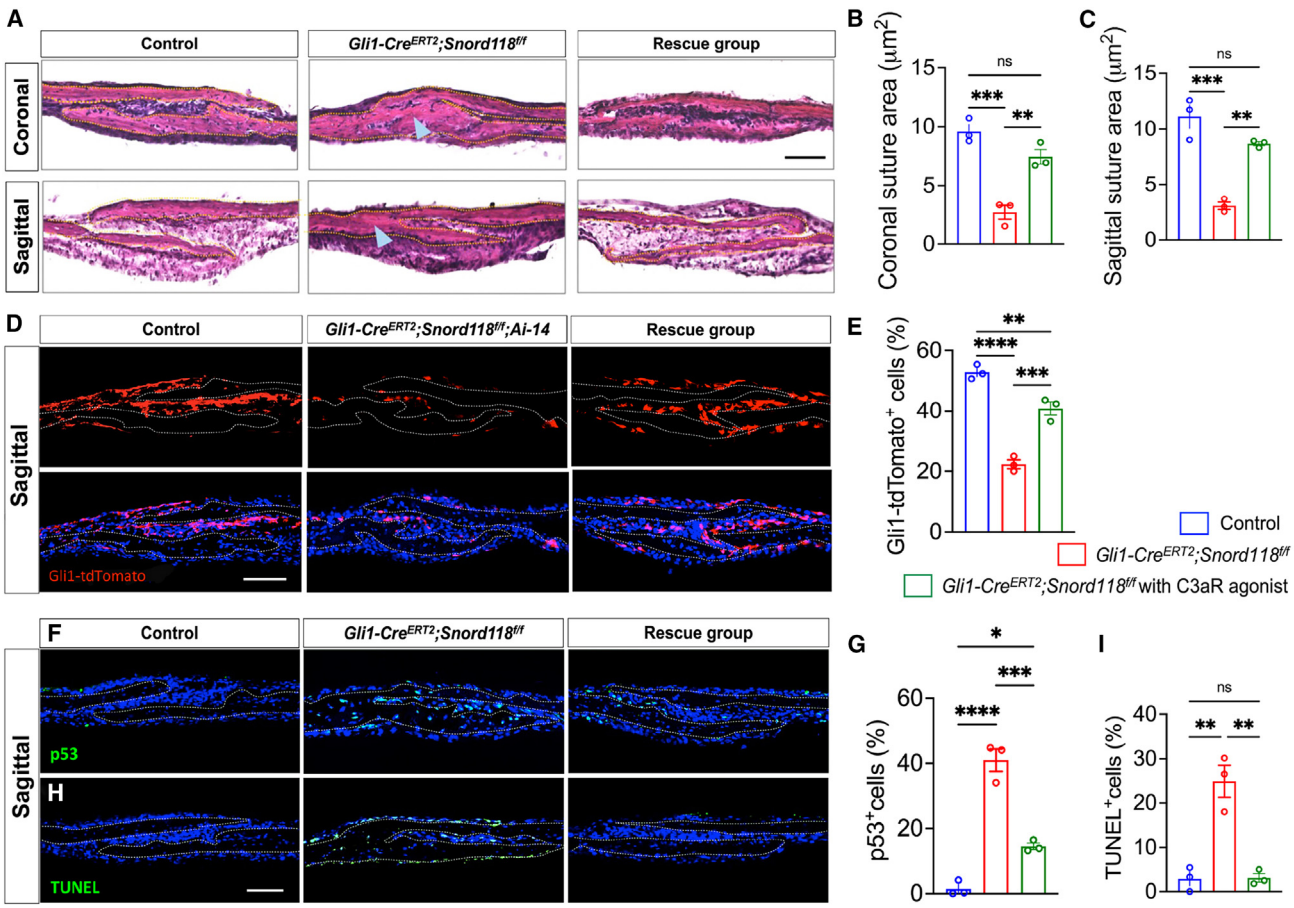

Figure 7. Complement pathway activation rescues suture defects in *Snord118* mutant suture explants

(A) H&E staining of coronal and sagittal sections of suture explants from control, *Gli1-Cre^{ERT2};Snord118$^{f/f}$*, and *Gli1-Cre^{ERT2};Snord118$^{f/f}$* mice treated with C3aR agonist (rescue group). Blue arrowheads indicate the area of bony fusion.

(B and C) Quantification of coronal and sagittal suture area of calvarial suture explants.

(D) IHC staining of Gli1-tdTomato in sagittal suture explants from control, *Gli1-Cre^{ERT2};Snord118$^{f/f}$;Ai-14*, and *Gli1-Cre^{ERT2};Snord118$^{f/f}$;Ai-14* mice treated with C3aR agonist.

(F and H) IHC staining of p53 and TUNEL staining in sagittal suture explants from control, *Gli1-Cre^{ERT2};Snord118$^{f/f}$* and *Gli1-Cre^{ERT2};Snord118$^{f/f}$* mice treated with C3aR agonist.

(E, G, and I) Quantification of the percentage of Gli1$^+$, p53$^+$, and TUNEL$^+$ cells per section. Scale bars, 100 μm. Values represent mean ± SEM with statistical significance assessed by one-way ANOVA with Tukey post hoc tests (n = 3 mice). *p < 0.05, **p < 0.01, ***p < 0.001, ****p < 0.0001; ns represents nonsignificant. Note: (B and C) Suture area was defined by the total area of suture mesenchyme in suture sections and quantified by ImageJ. Five to six sections per mouse were analyzed and averaged to represent the mean value from one mouse/sample. Each dot on graph quantification is one mouse (n = 3 mice per group).

ribosome biogenesis selectively regulates suture MSC fate via the complement pathway, disruption of which leads to suture growth and craniosynostosis defects.

Our study of ribosome biogenesis in suture MSCs is distinct from previous signaling and transcriptional research (Stanton et al., 2022). Protein synthesis and mRNA translation in stem and progenitor cells during tissue development are dynamic and sensitive to changes in ribosome biogenesis. Tight regulation of protein synthesis machinery, including ribosomes and their associated factors, is essential for stem cell self-renewal and differentiation (Saba et al., 2021). Our studies provide evidence that a global disruption of ribosome biogenesis selectively affects suture MSCs, which serve as the engine of calvarial growth, maintenance, and regeneration. Loss of suture MSCs is one of the major causes of craniosynostosis (Menon et al., 2021; Zhao et al., 2015). Our data revealed a significant decrease of Gli1$^+$ MSCs in the suture mesenchyme of *Snord118* mutant mice, which developed craniosynostosis. This Gli1$^+$ MSC loss is likely due to increased

p53 activation and subsequent apoptosis, which echo that perturbed ribosome homeostasis from unbalanced ribosome biogenesis causes p53 activation, leading to cell-cycle arrest and apoptosis (Golomb et al., 2014; Jones et al., 2008).

Ribosome biogenesis regulates MSC fate via multiple mechanisms, disruption of which contributes to craniosynostosis. Gli1$^+$ MSCs can give rise to osteoblasts, bone marrow adipocytes, and stromal cells. We found that tdTomato-labeled Gli1$^+$ mutant MSCs prematurely differentiate into osteoblast lineage cells labeled by Runx2 and Sp7. It is possible that ribosome biogenesis disruption abnormally upregulates activators of osteogenic differentiation. Alternatively, ribosome biogenesis disruption inhibits suppressors of osteogenic differentiation, which is illustrated by *Twist1* downregulation in mutant cranial sutures. Twist1 represses pro-osteogenic differentiation factor Runx2 to maintain mesenchymal cells in an undifferentiated state (Bialek et al., 2004). Twist1 downregulation is expected to relieve the repression of Runx2 and lead to premature osteogenic differentiation in *Snord118* mutant MSCs. Meanwhile, bone-resorbing cells named osteoclasts are reduced in *Snord118* mutant mice, which might result in more osteoblast cells contributing to premature suture fusion and craniosynostosis.

Our studies provide new insights into the regulation and function of the complement pathway in craniofacial biology and disease. The complement system drives inflammation and provides innate immune protection against infection (Hajishengallis et al., 2017). It has emerging roles in stem cells, tissue homeostasis, and injury repair (Rutkowski et al., 2010). Human mutations in complement pathway components selectively affect craniofacial structure and lead to 3MC syndrome (Mingarelli, Malpeuch, Michels, and Carnevale syndromes), which is characterized by facial dysmorphism, cleft lip/palate, and craniosynostosis (Munye et al., 2017; Rooryck et al., 2011). Our findings showed that *Snord118* KO mice have reduced expression of complement pathway components in cranial sutures coupled with craniosynostosis defects. Importantly, functional studies suggest that the complement pathway is a key mediator of *Snord118*-controlled ribosome biogenesis functions in regulating MSC fate, disruption of which might contribute to craniosynostosis in 3MC syndrome. Future research should investigate what cellular functions the complement pathway might have in suture growth. In this regard, complement factor C3a has been shown to play critical roles in neural crest cell migration (Carmona-Fontaine et al., 2011), disruption of which might occur in 3MC syndrome. It is also important to investigate how a global disruption of ribosome biogenesis selectively affects the complement pathway.

Our human iPSC-derived MSC model provides a valuable platform to study cranial suture development, disease pathogenesis, and potential treatments for craniofacial disorders. These iMSCs are capable of clonal self-renewal and multiple differentiation toward osteogenic, adipogenic, and chondrogenic cell fate. Human iPSC cells coupled with CRISPR-Cas9 genome editing cross-validated that *SNORD118* mutations cause MSC proliferation reduction and premature osteogenic differentiation, which is consistent with mouse genetic studies. Importantly, iMSCs can provide unlimited cell materials for cell-number demanding research such as ribosome profiling. This is shown by our combined ribosome profiling and bulk RNA-seq studies of control and mutant iMSCs, which led to the finding of complement pathway dysregulations caused by *Snord118* mutations. Future studies should directly compare human iPSC-derived MSCs with Gli1-tdTomato$^+$ cells from *Gli1-Cre^{ERT2};Ai-14* mice.

Overall, our study provides mechanistic insights into the specificity of ribosome biogenesis in craniofacial tissue development and diseases. Our human iPSC and mouse genetic studies cross-validated that suture MSCs are particularly sensitive to the disruption of global ribosome biogenesis, leading to changes in their cell fate. We reveal ribosome biogenesis-mediated regulation as well as critical functions of the complement pathway in suture MSC maintenance, which has implications for the pathogenesis of craniofacial defects in 3MC syndrome.

EXPERIMENTAL PROCEDURES

Resource availability

Corresponding author

Further information and requests for resources and reagents should be directed to and will be fulfilled by the lead contact, Jianfu Chen (jianfu@usc.edu).

Materials availability

All new reagents will be made available upon request for scientific research while a completed Materials Transfer Agreement may be required.

Data and code availability

All data reported in this paper will be shared by the lead contact upon request. This paper does not report original code. The RNA-seq data have been deposited to GEO under accession code GSE223614. The Riboseq data have been deposited to GEO under accession code GSE223615.

Experimental models and methods

Mouse models

Gli1-Cre^{ERT2} (JAX#007913), *tdTomato* (JAX#007905), and *C3ar1$^{-/-}$* (JAX#033904) mouse lines were obtained from Jackson Laboratory. For induction of Cre lines, tamoxifen (Sigma T5648) was suspended in corn oil (Sigma C8267) at 20 mg mL^{-1} and injected intraperitoneally at a dose of 1 mg per 10 g body weight for 2

consecutive days. Mice were injected with tamoxifen at postnatal day 20 (P20), and their calvarial bones were collected at the indicated time points. To examine the phenotype when Gli1$^+$ MSCs are more restricted to cranial sutures at a later stage, mice were injected with tamoxifen at 1 month old for 3 consecutive days. All mice were housed under a 12 h light/dark cycle with controlled temperature and humidity. Mice were euthanized via carbon dioxide overdose followed by cervical dislocation. All studies were performed with the approval of the Institutional Animal Care and Use Committee of the University of Southern California.

Human MSC induction and characterization

For neural crest cell (NCC) induction, hiPSCs were cultured to get confluence and were passaged by ReLeSR (STEMCELL Technologies) into cell clusters for suspension culture in the low attachment dish with the N2B27 medium containing DMEM/F12, Neurobasal, 1% N2, 2% B27, NEAA, GlutaMAX, 20 ng/mL bFGF, 20 ng/mL EGF, and 100 μg/ml Primocin. To improve NCC induction, the 10 μM SB431542 and 1 μM CHIR99021 (Selleckchem) were added to the medium. At day 10, the EBs were attached to the normal culture plate without any coating. The NCCs migrated from the EBs and attached to the plate. The NCCs were harvested manually on day 14 and cultured in the N2B27 medium with 20 ng/mL bFGF and 20 ng/mL EGF to form the maintenance culture. The hiPSC-derived NCCs were cultured in α-MEM containing 10% FBS to induce MSCs. The cell media were changed every other day and passaged every 4–5 days. At day 35 the cells became MSC-like cells and were cultured in α-MEM containing 10% FBS for further characterization.

The self-renewal of human iPSC-derived MSCs (iMSCs) was examined according to the published method. Briefly, iMSCs dissociated by Accutase were filtered, and about 1×10^4 single cells were seeded in an ultra-low attachment surface plate with α-MEM containing 25 μg/mL insulin, 20 ng/mL EGF, 20 ng/mL bFGF, 10 ng/ml TGF-b1, 1% N2 supplement, and 100 μg/mL Primocin for sphere formation. After 14 days, the spheres were dissociated by Accutase and seeded with the same number of cells as the single-cell suspension for the next passage. An EdU assay was performed by using the EdU Cell Proliferation Kit (Click Chemistry Tools); 10 μM EdU was used to treat cells for 2 h before fixing the samples. For osteogenesis, the StemPro Osteogenesis Differentiation medium (Thermo) was used to culture iMSCs. The medium was changed every 2 days. The cells were fixed by 4% PFA at day 21 and then stained by 2% Alizarin Red S solution. For adipogenesis, the StemPro Adipogenesis Differentiation Kit (Thermo) was used according to the manufacturer, and 0.5% Oil Red O solution was stained on the differentiated cells at day 14. For chondrogenesis, the cells were dissociated to generate micromass cultures, followed by seeding 5-μL droplets of cell solution (2×10^7 cells/mL) in the center of 24-well plate wells. After cultivating micromass cultures for 2 h, the StemPro Chondrogenesis Differentiation Medium (Thermo) was added to the plate and was changed every 2 days. The cells were fixed by 4% PFA at day 14 and stained by 1% Alcian blue solution.

SUPPLEMENTAL INFORMATION

Supplemental information can be found online at https://doi.org/10.1016/j.stemcr.2023.10.015.

ACKNOWLEDGMENTS

We thank the Chen laboratory colleagues for stimulating discussions. We are grateful for Jotham Sadan's critical reading of the manuscript. This study was supported by grants R01DE030901 (J.C.), R21AG075665 (J.C.), and R21AG070681 (J.C.) from the National Institutes of Health.

AUTHOR CONTRIBUTIONS

S.J., J.H.B., W.Z., and M.J.Z. performed all experiments. J.H.B, analyzed all bioinformatic data. S.J, and Z.P.L, helped with the manuscript writing. J.F.C. designed and interpreted the experiments and wrote the manuscript.

DECLARATION OF INTERESTS

The authors declare no competing interests.

Received: April 10, 2023
Revised: October 22, 2023
Accepted: October 23, 2023
Published: November 16, 2023

REFERENCES

Bajpai, R., Chen, D.A., Rada-Iglesias, A., Zhang, J., Xiong, Y., Helms, J., Chang, C.-P., Zhao, Y., Swigut, T., and Wysocka, J. (2010). CHD7 cooperates with PBAF to control multipotent neural crest formation. Nature *463*, 958–962. https://doi.org/10.1038/nature08733.

Bialek, P., Kern, B., Yang, X., Schrock, M., Sosic, D., Hong, N., Wu, H., Yu, K., Ornitz, D.M., Olson, E.N., et al. (2004). A Twist Code Determines the Onset of Osteoblast Differentiation. Dev. Cell *6*, 423–435. https://doi.org/10.1016/s1534-5807(04)00058-9.

Carmona-Fontaine, C., Theveneau, E., Tzekou, A., Tada, M., Woods, M., Page, K.M., Parsons, M., Lambris, J.D., and Mayor, R. (2011). Complement Fragment C3a Controls Mutual Cell Attraction during Collective Cell Migration. Dev. Cell *21*, 1026–1037. https://doi.org/10.1016/j.devcel.2011.10.012.

Faal, T., Phan, D.T.T., Davtyan, H., Scarfone, V.M., Varady, E., Blurton-Jones, M., Hughes, C.C.W., and Inlay, M.A. (2019). Induction of Mesoderm and Neural Crest-Derived Pericytes from Human Pluripotent Stem Cells to Study Blood-Brain Barrier Interactions. Stem Cell Rep. *12*, 451–460. https://doi.org/10.1016/j.stemcr.2019.01.005.

Farley-Barnes, K.I., Ogawa, L.M., and Baserga, S.J. (2019). Ribosomopathies: Old Concepts, New Controversies. Trends Genet. *35*, 754–767. https://doi.org/10.1016/j.tig.2019.07.004.

Golomb, L., Volarevic, S., and Oren, M. (2014). p53 and ribosome biogenesis stress: The essentials. FEBS Lett. *588*, 2571–2579. https://doi.org/10.1016/j.febslet.2014.04.014.

Hajishengallis, G., Reis, E.S., Mastellos, D.C., Ricklin, D., and Lambris, J.D. (2017). Novel mechanisms and functions of complement. Nat. Immunol. *18*, 1288–1298. https://doi.org/10.1038/ni.3858.

Hetman, M., and Slomnicki, L.P. (2019). Ribosomal biogenesis as an emerging target of neurodevelopmental pathologies. J. Neurochem. *148*, 325–347. https://doi.org/10.1111/jnc.14576.

Holmes, G., Gonzalez-Reiche, A.S., Lu, N., Zhou, X., Rivera, J., Kriti, D., Sebra, R., Williams, A.A., Donovan, M.J., Potter, S.S., et al. (2020). Integrated Transcriptome and Network Analysis Reveals Spatiotemporal Dynamics of Calvarial Suturogenesis. Cell Rep. *32*, 107871. https://doi.org/10.1016/j.celrep.2020.107871.

Ingolia, N.T., Hussmann, J.A., and Weissman, J.S. (2019). Ribosome Profiling: Global Views of Translation. Cold Spring Harbor Perspect. Biol. *11*, a032698. https://doi.org/10.1101/cshperspect.a032698.

Jenkinson, E.M., Rodero, M.P., Kasher, P.R., Uggenti, C., Oojageer, A., Goosey, L.C., Rose, Y., Kershaw, C.J., Urquhart, J.E., Williams, S.G., et al. (2016). Mutations in SNORD118 cause the cerebral microangiopathy leukoencephalopathy with calcifications and cysts. Nat. Genet. *48*, 1185–1192. https://doi.org/10.1038/ng.3661.

Jones, N.C., Lynn, M.L., Gaudenz, K., Sakai, D., Aoto, K., Rey, J.-P., Glynn, E.F., Ellington, L., Du, C., Dixon, J., et al. (2008). Prevention of the neurocristopathy Treacher Collins syndrome through inhibition of p53 function. Nat. Med. *14*, 125–133. https://doi.org/10.1038/nm1725.

Kajdic, N., Spazzapan, P., and Velnar, T. (2018). Craniosynostosis - Recognition, clinical characteristics, and treatment. Bosn. J. Basic Med. Sci. *18*, 110–116. https://doi.org/10.17305/bjbms.2017.2083.

Khajuria, R.K., Munschauer, M., Ulirsch, J.C., Fiorini, C., Ludwig, L.S., McFarland, S.K., Abdulhay, N.J., Specht, H., Keshishian, H., Mani, D.R., et al. (2018). Ribosome Levels Selectively Regulate Translation and Lineage Commitment in Human Hematopoiesis. Cell *173*, 90–103.e19. https://doi.org/10.1016/j.cell.2018.02.036V.

Kiss, T., Fayet, E., Jády, B.E., Richard, P., and Weber, M. (2006). Biogenesis and Intranuclear Trafficking of Human Box C/D and H/ACA RNPs. Cold Spring Harb Sym *71*, 407–417. https://doi.org/10.1101/sqb.2006.71.025.

Kufel, J., and Grzechnik, P. (2019). Small Nucleolar RNAs Tell a Different Tale. Trends Genet. *35*, 104–117. https://doi.org/10.1016/j.tig.2018.11.005.

Liu, Q., Shvarts, T., Sliz, P., and Gregory, R.I. (2020). RiboToolkit: an integrated platform for analysis and annotation of ribosome profiling data to decode mRNA translation at codon resolution. Nucleic Acids Res. *48*, W218–W229. https://doi.org/10.1093/nar/gkaa395.

Maruyama, T., Jeong, J., Sheu, T.-J., and Hsu, W. (2016). Stem cells of the suture mesenchyme in craniofacial bone development, repair and regeneration. Nat. Commun. *7*, 10526. https://doi.org/10.1038/ncomms10526.

Menon, S., Salhotra, A., Shailendra, S., Tevlin, R., Ransom, R.C., Januszyk, M., Chan, C.K.F., Behr, B., Wan, D.C., Longaker, M.T., and Quarto, N. (2021). Skeletal stem and progenitor cells maintain cranial suture patency and prevent craniosynostosis. Nat. Commun. *12*, 4640. https://doi.org/10.1038/s41467-021-24801-6.

Mills, E.W., and Green, R. (2017). Ribosomopathies: There's strength in numbers. Science *358*, eaan2755. https://doi.org/10.1126/science.aan2755.

Mödinger, Y., Löffler, B., Huber-Lang, M., and Ignatius, A. (2018). Complement involvement in bone homeostasis and bone disorders. Semin. Immunol. *37*, 53–65. https://doi.org/10.1016/j.smim.2018.01.001.

Munye, M.M., Diaz-Font, A., Ocaka, L., Henriksen, M.L., Lees, M., Brady, A., Jenkins, D., Morton, J., Hansen, S.W., Bacchelli, C., et al. (2017). COLEC10 is mutated in 3MC patients and regulates early craniofacial development. PLoS Genet. *13*, e1006679. https://doi.org/10.1371/journal.pgen.1006679.

Nakashima, K., Zhou, X., Kunkel, G., Zhang, Z., Deng, J.M., Behringer, R.R., and de Crombrugghe, B. (2002). The Novel Zinc Finger-Containing Transcription Factor Osterix Is Required for Osteoblast Differentiation and Bone Formation. Cell *108*, 17–29. https://doi.org/10.1016/s0092-8674(01)00622-5.

Neben, C.L., Idoni, B., Salva, J.E., Tuzon, C.T., Rice, J.C., Krakow, D., and Merrill, A.E. (2014). Bent bone dysplasia syndrome reveals nucleolar activity for FGFR2 in ribosomal DNA transcription. Hum. Mol. Genet. *23*, 5659–5671. https://doi.org/10.1093/hmg/ddu282.

Peculis, B.A., and Steitz, J.A. (1993). Disruption of U8 nucleolar snRNA inhibits 5.8S and 28S rRNA processing in the Xenopus oocyte. Cell *73*, 1233–1245. https://doi.org/10.1016/0092-8674(93)90651-6.

Rooryck, C., Diaz-Font, A., Osborn, D.P.S., Chabchoub, E., Hernandez-Hernandez, V., Shamseldin, H., Kenny, J., Waters, A., Jenkins, D., Kaissi, A.A., et al. (2011). Mutations in lectin complement pathway genes COLEC11 and MASP1 cause 3MC syndrome. Nat. Genet. *43*, 197–203. https://doi.org/10.1038/ng.757.

Rutkowski, M.J., Sughrue, M.E., Kane, A.J., Ahn, B.J., Fang, S., and Parsa, A.T. (2010). The complement cascade as a mediator of tissue growth and regeneration. Inflamm. Res. *59*, 897–905. https://doi.org/10.1007/s00011-010-0220-6.

Saba, J.A., Liakath-Ali, K., Green, R., and Watt, F.M. (2021). Translational control of stem cell function. Nat. Rev. Mol. Cell Biol. *22*, 671–690. https://doi.org/10.1038/s41580-021-00386-2.

Stanton, E., Urata, M., Chen, J.-F., and Chai, Y. (2022). The clinical manifestations, molecular mechanisms and treatment of craniosynostosis. Dis. Model. Mech. *15*, dmm049390. https://doi.org/10.1242/dmm.049390.

Stebbins, M.J., Gastfriend, B.D., Canfield, S.G., Lee, M.-S., Richards, D., Faubion, M.G., Li, W.-J., Daneman, R., Palecek, S.P., and Shusta, E.V. (2019). Human pluripotent stem cell–derived brain pericyte–like cells induce blood-brain barrier properties. Sci. Adv. *5*, eaau7375. https://doi.org/10.1126/sciadv.aau7375.

Stepanov, G.A., Filippova, J.A., Komissarov, A.B., Kuligina, E.V., Richter, V.A., and Semenov, D.V. (2015). Regulatory Role of Small Nucleolar RNAs in Human Diseases. BioMed Res. Int. *2015*, 206849. https://doi.org/10.1155/2015/206849.

Yahara, Y., Nguyen, T., Ishikawa, K., Kamei, K., and Alman, B.A. (2022). The Origins and Roles of Osteoclasts in Bone Development, Homeostasis and Repair. Development *149*. https://doi.org/10.1242/dev.199908.

Yelick, P.C., and Trainor, P.A. (2015). Ribosomopathies: Global process, tissue specific defects. Rare Dis. *3*, e1025185. https://doi.org/10.1080/21675511.2015.1025185.

Yu, M., Ma, L., Yuan, Y., Ye, X., Montagne, A., He, J., Ho, T.-V., Wu, Y., Zhao, Z., Sta Maria, N., et al. (2021). Cranial Suture Regeneration Mitigates Skull and Neurocognitive Defects in Craniosynostosis. Cell *184*, 243–256.e18. https://doi.org/10.1016/j.cell.2020.11.037.

Zhao, H., Feng, J., Ho, T.-V., Grimes, W., Urata, M., and Chai, Y. (2015). The suture provides a niche for mesenchymal stem cells of craniofacial bones. Nat. Cell Biol. *17*, 386–396. https://doi.org/10.1038/ncb3139.